Journal of Solid Mechanics Vol. 6, No. 4 (2014) pp. 378-388

A Cohesive Zone Model for Crack Growth Simulation in AISI 304 Steel

F. Javidrad *, M. Mashayekhy

Center for Postgraduate Studies, Aeronautical University of Science and Technology, Tehran, Iran

Received 15 July 2014; accepted 20 September 2014

ABSTRACT

Stable ductile crack growth in 3 mm thick AISI 304 stainless steel specimens has been investigated experimentally and numerically. Multi-linear Isotropic Hardening method coupled with the Von-Mises yield criterion was adopted for modeling elasto-plastic behavior of the material. Mode-I CT fracture specimens have been tested to generate experimental load-displacement-crack growth data during stable crack growth. The critical fracture energy (J_{Ic}) was then determined using the finite elements results in conjunction with the experimental data. The effect of in-plane constraints on the numerical-experimental J_{Ic} calculation was then investigated. The results of finite element solution were used to tailor an exponential CZM model for simulation of mode-I stable crack growth in CT specimens. It is found that the adopted CZM is generally insensitive to the applied constraints to the crack tip stress state and thus it can effectively be used for simulating crack growth in this material.

Keywords: Cohesive zone model; Finite element; CT specimen; In-plane constraint; AISI 304 steel.

1 INTRODUCTION

DUCTILE fracture processes are fairly common to failures in structural components. In many practical structural design cases, a great deal of effort has been made to prevent fracture in structural components. Aircraft structures, ship structures, bridges, pressure vessels and line pipe materials are all designed against fracture at working temperatures. The most important tool for such a design is an effective crack growth simulation technique together with a reliable crack growth criterion. In practice, it is common to consider ductile crack growth in a form of crack propagation resistant curve (R-curve), with crack growth expressed as a function of either crack tip parameters like the stress intensity factor (K), energy dissipation rates (J-integral) or crack tip opening displacement (CTOD) [1-2]. There are, of course, some other crack growth criteria suggested for characterization of ductile fracture in metals [3]. Among them, the crack tip opening angle (CTOA) [4] is the most popular crack growth criterion used in practice. Unfortunately, dependency of the CTOA and CTOD results to the in-plane constraints at the crack tip is not well understood yet.

Damage mechanics based models are alternative approaches that are being increasingly used. A major advantage of the numerical damage mechanics models is that they do not basically need an initial crack present in the component. In addition, the transferability of toughness data from specimens to structures are handled much better

* Corresponding author. Tel.: +98 21 33341541.
E-mail address: f_javidrad@yahoo.com (F. Javidrad).

in damage mechanics models [5]. However, there are some difficulties in using these methods, such as mesh size sensitivity, mesh adaptation and stability of numerical solutions [6].

The concept of the cohesive zone model (CZM) which was first proposed by Barrenblatt [7] and Dugdale [8] is now considered as a powerful damage mechanics approach to analyze fracture process. The CZM has been previously used to model stable fracture process in a number of materials including polymers [9], metals [10], ceramic materials [11], bi-material systems [12], concrete [13], functionally graded materials [14] and woven and laminated composite materials [15-17]. Besides, the CZM can be assumed rate-dependent to simulate dynamic crack growth in solid materials [18].

Even though the CZM has been widely used in ductile fracture, it is not yet clearly understood how to calculate CZM properties. Therefore, the main objective of the present work is to identify CZM parameters for AISI304 steel plates using an experimental calibration method. AISI 304 is a ductile stainless steel that found many applications in industries. Mode-I fracture is considered in this study since it is more often seen in failure of fracture-critical structures such as pressure tanks. The elasto-plastic finite element crack growth simulation in compact tension (CT) specimens was carried out to tailor a CZM model for this material. The presented work involves:

- Conducting tensile tests to get material behavior including the stress-strain curve,
- Conducting CT fracture tests to investigate stable crack growth in AISI 304 steel under static loading for mode-I fracture,
- Determining critical J-integral using a numerical/experimental method,
- Identifying CZM parameters using numerical simulation to represent the crack growth in this material under static loading.

2 BASIS OF THE CZM

When a cracked material is subjected to a load, energy dissipation occurs. The energy dissipation is mainly due to microcracking and localized deformation of the material which generally takes place in a small region called fracture process zone. This makes the material globally exhibit strain softening, i.e. a negative slope of the stress-strain diagram. The behavior of the material outside this region can still be linear elastic. If the size of the fracture process zone is large enough as compared to the crack length, linear elastic fracture mechanics assumptions will not be further applicable. One method frequently used to simplifying fracture process zone behavior modeling is concentrating the fracture process zone at the crack tip and then characterizing it in the form of a stress-displacement which exhibit softening. This method is usually referred to as cohesive crack model.

CZM first introduced in 1960 to account for the basic aspects of the nonlinear material behavior ahead of the tip of a pre-existing crack. In this procedure, the crack is assumed to extend and to open while still transferring stress from one face to the other. To implement the CZM to a finite element model, cohesive elements are inserted at the interfaces of continuum elements. Whereas these interface elements obey a special traction-stress law. The material outside is described by conventional constitutive equations. Decohesion law actually relates surface tractions to the relative displacement or separation at an interface, where a crack may occur. These tractions generally consist of one normal and two tangential components, compatible with crack opening displacement mode. Crack or damage initiation is related to an interfacial strength, i.e. the maximum traction on the traction separation curve. When the area under this curve is equal to critical fracture energy, the traction is reduced to zero and new crack surfaces are formed.

Fig. 1 shows schematically the Mode-I fracture of a material which is described by the cohesive normal traction (T_n) as a function of relative displacements (δ) between two faces. In general:

$$T_n = f(\delta) \tag{1}$$

where f is a function used to describe stress distribution along the crack faces at the cohesive zone [19]. In this model, it is assumed that all micro-structural mechanisms of the fracture process can be captured by two cohesive parameters, *i*) the maximum traction or cohesive strength, $\sigma_{\max}$, and *ii*) a critical separation, δ_0 , beyond which the respective cohesive layer has lost its stress carrying capacity and the crack extends (or δ_n , the separation at the point of maximum traction). Alternatively, the separation energy, G_c, being the area under the $f(\delta)$ curve, as given in Eq. (2) , can be used as a cohesive parameter.

$$G_c = \int_0^{\delta_0} f(\delta)\, d\delta \tag{2}$$

There are many traction-separation models introduced in the literature. As it is implied previously, cohesive zone debonding generally allows three modes of separation, mode-I (opening), mode-II (shearing), mode-III (tearing) and mixed-mode displacements. The various traction-separation models for mode-I fall in three main categories, as shown schematically in Fig. 2. Some of the most popular models with a brief description of their applications are given in Table 1.

Unlike the traditional finite element (FE) method, cohesive elements are inserted between the discretized elements. Decohesion process is then controlled via attributing special traction-separation behavior to these interface elements. Although the CZM incorporating FE method is known as a powerful method for quantifying crack growth in various materials, there are still some difficulties in using CZM for simulation of crack growth. Determining suitable material parameters, difficulties in mesh and FE modeling and problems in prediction of crack growth direction, specifically for arbitrary curved crack extension path, are examples of such difficulties associated with this method.

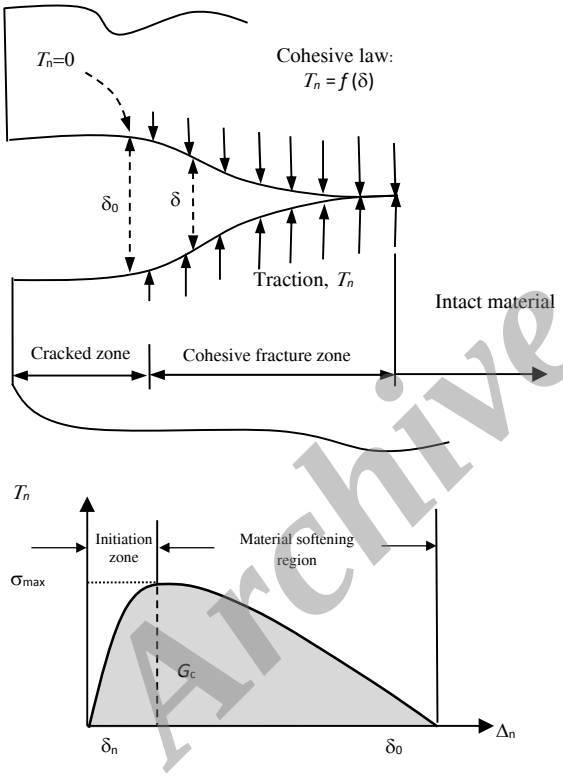

Fig. 1
Schematic of cohesive model (damage is localized at the interface) and a typical stress-traction variation at the interface.

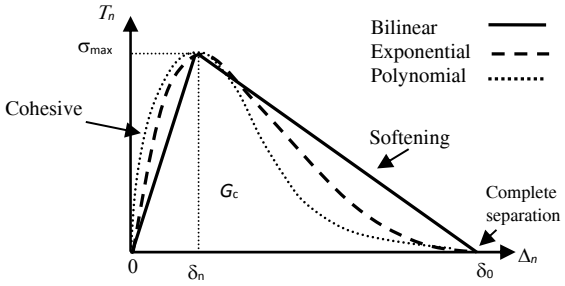

Fig. 2
Three common categories of traction-separation laws.

Table 1
The most popular cohesive zone models

Model name	Traction-separation curve schematic	Traction-separation and separation energy relationships	Applications
Linear	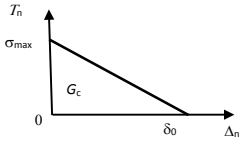	$T_n = \sigma_{\max}(1-\frac{\Delta_n}{\delta_0}) \quad \Delta_n \le \delta_0 \; [0,1]$ $G_c = \frac{1}{2}\delta_0 \sigma_{\max}$	Brittle materials and crack growth modeling in concrete. Fracture load prediction in structures under the linear elastic fracture mechanics assumptions [20].
Polynomial model (Scheider and Brocks [21])	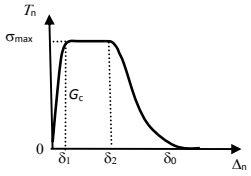	$T_n = \sigma_{\max} \cdot \begin{cases} 2\left(\frac{\Delta_n}{\delta_1}\right)-\left(\frac{\Delta_n}{\delta_1}\right)^2 & \Delta_n < \delta_1 \\ 1 & \delta_1 \le \Delta_n < \delta_2 \\ 2\left(\frac{\Delta_n-\delta_2}{\delta_0-\delta_2}\right)^3 - 3\left(\frac{\Delta_n-\delta_2}{\delta_0-\delta_2}\right)^2 + 1 & \delta_2 \le \Delta_n < \delta_0 \end{cases}$ $G_c = \frac{1}{2}\sigma_{\max}.\delta_0\left(1-\frac{2}{3}\frac{\delta_1}{\delta_0}+\frac{\delta_2}{\delta_0}\right)$	Thin sheets of aluminium materials, Crack growth simulation in aircraft stiffened panel [22]
Exponential model	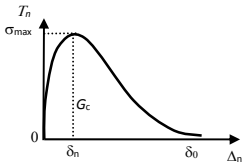	$T_n = \sigma_{\max}\left(\frac{\Delta_n}{\delta_n}\right).e^{1-\Delta_n/\delta_n}$ $G_c = e.\sigma_{\max}.\delta_n$	Thin sheet metals, Crack simulations in thin shells with out-of-plane deformations [23], Multi-site damage (MSD) analysis [24]
Gurson-Tvergaard-Needleman (GTN Model) [25]	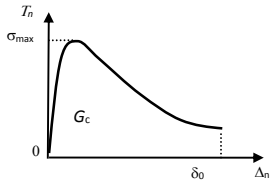	$T_n = \sigma_{\max}.ez\frac{\Delta_n}{\delta_0}.e^{-z(\Delta_n/\delta_0)}$, $e = \exp(1),\; z = 16e/9$ $G_c = \frac{9}{16}\sigma_{\max}\delta_0$	Analysis of ductile fracture in solids [26], Fracture modeling in thin sheets, Modeling slant cracks [27]. Pourous plastic material modeling [28]
Bilinear Model	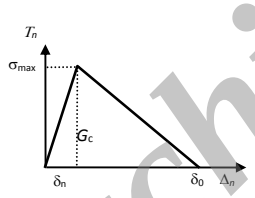	For Mode-I (δ_n >0): $T_n = \begin{cases} \frac{\sigma_{\max}}{\delta_n}\Delta_n & \Delta_n \le \delta_n \\ \frac{\sigma_{\max}}{\delta_n-\delta_0}.(\Delta_n-\delta_0) & \Delta_n > \delta_n \end{cases}$ $G_c = \sigma_{\max}.\delta_0/2$	Mode-I, Mode II and mixed mode I/II fracture in metals, compositesetc. [21], Delamination in laminated composites [29]
Trapezoidal (or Trilinear) Model	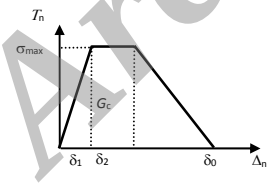	$T_n = \begin{cases} \left(\frac{\sigma_{\max}}{\delta_1}\right).\Delta_n & \Delta_n < \delta_1 \\ \sigma_{\max} & \delta_1 \le \Delta_n \le \delta_2 \\ \left(\frac{\sigma_{\max}}{\delta_0-\delta_2}\right).(\delta_0-\Delta_n) & \Delta_n > \delta_2 \end{cases}$ $G_c = \frac{1}{2}\sigma_{\max}(\delta_0+\delta_2-\delta_1)$	Local plasticity effects at the crack tip, (it is suitable for brittle materials). Mode II failure of bonded joints [30], Bone Fracture Characterization [31], Delamination growth modeling in laminated composites [32].

3 EXPERIMENTAL WORK

In order to determine a suitable model for crack growth in a material, it is first necessary to identify its strength properties. These properties are tensile strength and fracture strength parameters.

3.1 Tensile test

The investigated sheets are 3 mm thick and made of AISI 304 stainless steel. AISI 304 stainless steel is a very good corrosion resistance material. Besides, it has good resistance to oxidation in intermittent services up to 870 ˚C. It has

also good machinability characteristics which make them attractive for use in many industries such as nuclear power plants. The material essentially contains 0.08% C, 18% Cr and 10% Ni.

Specimens were cut from a sheet panel in LT and TT directions according to ASTM E8-04 standard. Tensile tests were carried out as ASTM E8-04 standard procedure utilizing a 15 T tensile test machine. The average test results are given in Table 2. No distinct difference in tensile behavior was observed in LT and TT directions. Therefore, orientation dependence regarding yield strength is considered to be negligible for this material. The rupture surface in all specimens was perpendicular to the load line. A typical stress-strain variation during test is also given in Fig. 3.

3.2 CT fracture test

The fracture properties required for this study were determined by experiments performed on CT specimens. Twelve CT specimens and the required fittings and anti-buckling plates were produced according to the ASTM E 2472-06 standard. Dimensions of the specimens in accordance with this standard are shown in Fig. 4.

The specimens were loaded quasi-statically such that to produce stress intensity factor rate between 0.2 MPa$\sqrt{}$m/sec and 3 MPa$\sqrt{}$m/sec. Using stress intensity factor relation for this specimen (Eq. (3)), the proper loading rate is determined.

$$K_I = \frac{P}{B\sqrt{a}} f(a/W) \tag{3}$$

where K_I denotes mode-I stress intensity factor, P is the applied load, B is the specimen thickness, a is the initial crack length and $f(a/W)$ is a correction factor expressed as:

$$f(a/W) = 0.2960(a/W) - 1.855(a/W)^2 + 6.557(a/W)^3 - 10.17(a/W)^4 + 6.389(a/W)^5 \tag{4}$$

An accurate scale was carved along the crack line to aid in measuring crack length during growth. The crack growth was followed using a digital microscope which was mounted on a movable stand. Values of loads have been taken from the test machine load cell which was accurately calibrated prior to test. Displacement data have been measured by an extensometer and a clip gauge. The crack length data were determined by image correlation using Screen Maker v.2.31 software. A typical experimental load-applied displacement and crack length-applied displacement curves are exhibited in Fig. 5.

Table 2
Experimental stress-strain data for the AISI 304 material

Modulus of lasticity, E (Gpa)	208
Yield strength, σ_y (Mpa)	282
Ultimate tensile strength, σ_u (Mpa)	736

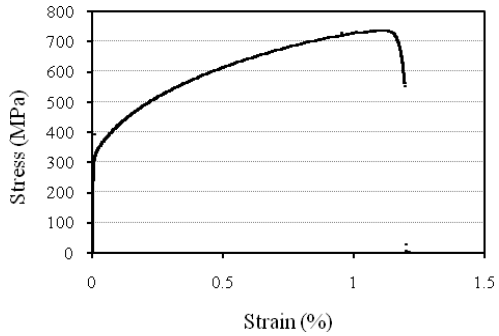

Fig. 3
A typical stress-strain variation during tensile test for the AISI 304 steel material.

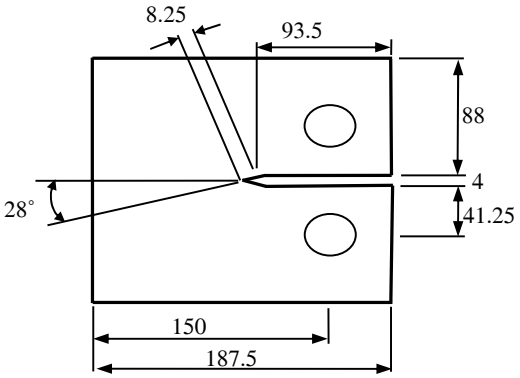

Fig. 4
Dimensions of the CT specimen in accordance with ASTM 2472-06. (dimensions in millimeter)

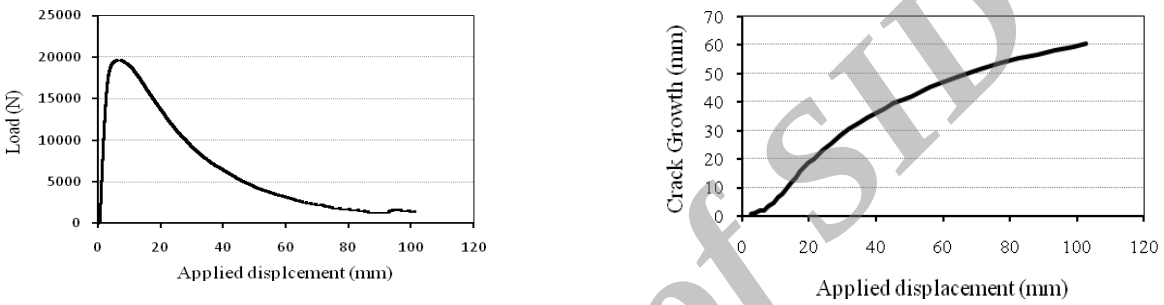

Fig. 5
Experimental load-applied displacement and crack growth-applied displacement data for AISI 304 steel material.

4 COHESIVE ZONE MODELING

The traction-separation relation for a mode-I crack is generally characterized using a scalar surface potential Φ by setting

$$T_n = \frac{\partial \Phi}{\partial \Delta_n} \tag{5}$$

where T_n denotes continuum normal traction and Δ_n is the normal separation between two surfaces of cohesive zone. The surface potential Φ actually represents the energy needed to separate the interface, i.e. separation between two surfaces of cohesive zone. If a proper potential function Φ is available, the constitutive equation between the cohesive traction and the relative separation can be derived. A number of different functions have been suggested to approximate Φ. In this study, an exponential potential function for mode-I fracture as suggested by Xu and Needleman [33] is employed.

$$\Phi(\Delta_n) = e\sigma_{\max}\delta_n\left(1-\left(1+\frac{\Delta_n}{\delta_n}\right)e^{-\frac{\Delta_n}{\delta_n}}\right) \tag{6}$$

where e is $exp(1)$, $\sigma_{\max}$ is the maximum stress, δ_n is the separation of interface elements at the maximum stress as given in Table 1. By differentiating the surface potential, the traction-separation relation is determined as:

$$T_n = e\sigma_{\max}\frac{\Delta_n}{\delta_n}e^{-\frac{\Delta_n}{\delta_n}} \tag{7}$$

The work of separation can be determined using Eq. 2. It is worth noting that in this model , T_n approaches zero at a very large value of δ_0 .

$$G_c = e\sigma_{\max}\delta_n \tag{8}$$

5 FE SIMULATION

5.1 Simulation of the tensile test

To obtain a proper material model and stress state for elastic-plastic behavior of the specimen, the tensile test specimen has been discretized by finite elements. ANSYS, Ver. 13 general purpose finite element software was employed. The FE model consists of 883 2D four-noded quadrilateral elements with 1000 nodes. Multi-linear Isotropic Hardening model was used to characterize the material behavior. The hardening rule actually describes the change in the yield surface with progressive yielding, so that the conditions for subsequent yielding can be established. In isotropic (or work) hardening, the yield surface remains centered about its initial centerline and expands in size as the plastic strains develop. The Multi-linear term in the method is referred to the description of the stress-strain behavior used to model the material. The elastic region in this material model is represented by a line while the plastic region is represented by some pieces of lines with different slopes, as shown in Fig. 6. This method, which is suitable for large strain problems, basically uses Von-Mises yield criterion coupled with an isotropic work hardening. Fig. 7 shows the simulation results using both plane stress (low constraint) and plane strain stress (full constraint) states. It is seen that the plane strain assumption fairly matches with the experimental results.

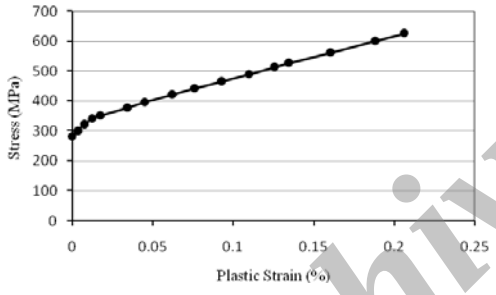

Fig. 6
Stress- plastic strain curve given for the Multi-linear Isotropic Work Hardening model.

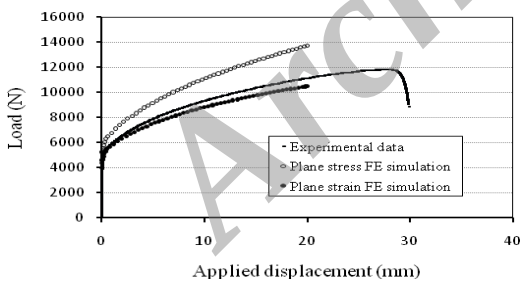

Fig. 7
Elasto-plastic FE simulation of the tensile test specimen.

5.2 Simulation of the CT test

The produced FE mesh using 2D elements is shown in Fig. 8. The FE model consists of 6969 four-noded elements with 14626 active degrees of freedom. The loading pins were also modeled by a high stiffness solid material including contact elements between the pin and the loading holes surfaces.

Three stress states: plane stress, plane strain and plane strain core were examined. In plane strain core analysis, a band of plane strain elements located around the crack tip while the rest of elements are plane stress elements. The half core height of the plane strain band was set equal to the thickness of the plate, as recommended in [34]. It is noted that each of the above stress states actually applies constraints with different degrees to the crack tip and therefore, can have different effects on the elasto-plastic behavior of the material at the crack tip region. (Some

researchers reported that the plane strain core assumptions generally gives a better results in stable ductile crack growth modeling in CT specimens, because of its ability to capturing stress triaxiality around the crack tip (for example see [35]).) FE model of the CT specimen in different crack lengths, from 5 to 102 *mm* of crack extension, was analyzed in several steps. In each crack length, the load on the specimen was determined from the experimental data, as given in Fig. 5, and the corresponding *J*-integral was calculated along a contour around the crack tip. The results, as presented in Fig. 9, show a strong R-curve exists in the fracture energy variation.

To verify validity of the calculated critical *J*, simulation of loading the specimen at a crack length, say 5 mm crack extension, has been performed by the adopted elasto-plastic FE analysis. The area under the simulated load-displacement results assuming plane strain state, as shown in Fig. 10, is then calculated using the Simpson rule for numerical integration. Finally, the critical J was calculated using Eq.(9) (see ASTM E-813-81).

$$J = \frac{A}{Bb} f(a_0 / W) \tag{9}$$

where A denotes area under the load-displacement curve, B represents the plate thickness, b is the uncracked ligament and f (a_0/W) is a correction factor equal to 2.2 for plane strain condition. The calculated value for the critical *J*-integral was 202.49 N/mm. For comparison purposes, values of the critical *J*-integral obtained by various methods for the 5 mm crack extension have been summarized in Table 3.

The critical *J*-integral at the initial crack length (J_{Ic}), which is needed for the CZM crack growth modeling, was finally determined using a graphical procedure as described in ASTM E-813-81.

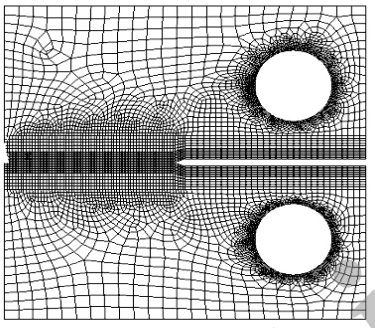

Fig. 8
Schematic of the CT specimen FE model.

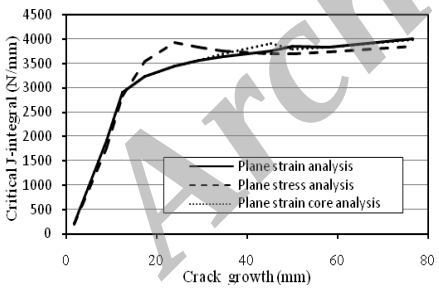

Fig. 9
Variation of the critical J-integral versus crack extension.

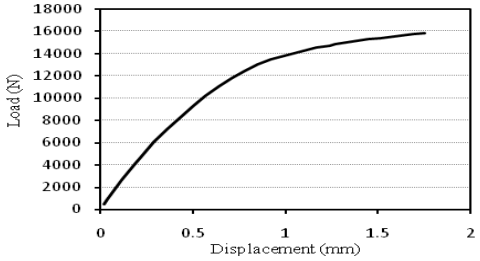

Fig. 10
FE-determined load-displacement variation at the crack extension of 5 mm.

6 CZM MODELING OF CRACK GROWTH

Typically, there are two methods for implementing CZM in finite element analysis of a cracked member: interface elements and bonded contact elements. Interface elements are zero thickness elements specially designed to represent cohesive zone between the components and to account for the separation across the interface. In this method, elements are meshed in between layers and linear or nonlinear material law for elasticity and debonding are defined. In bonded contact method, first general surface to surface contact constraint is used. Then, a specific traction separation material law is defined. When debonding occurs, usual contact behavior is implemented.

As it is stated previously and shown in Fig. 2, constitutive equations of a CZM include a representation of cohesive and softening branches, which causes the problem be strongly nonlinear. Thus, the development and implementation of a suitable solution algorithm is an important issue. In this study, an arc-length control combined with a Newton-Raphson algorithm for iterative solution of nonlinear equations is employed [36].

Table 3
Values of the critical J-integral at the crack extension of 5 mm

	Plane strain	Plane stress	Using Eq. (9)
Critical *J* (N/mm)	196.56	217.42	202.49

Table 4
Trial values of the cohesive strengths and their corresponding separation values.

Relative cohesive strength ($\sigma_{\max}/\sigma_y$)	Cohesive normal strength ($\sigma_{\max}$) (Mpa)	Interface separation (δ_n) (mm)
1.00	282.0	3.53
1.50	423.0	2.35
1.60	451.0	2.21
1.75	493.5	2.02
2.00	564.00	1.76

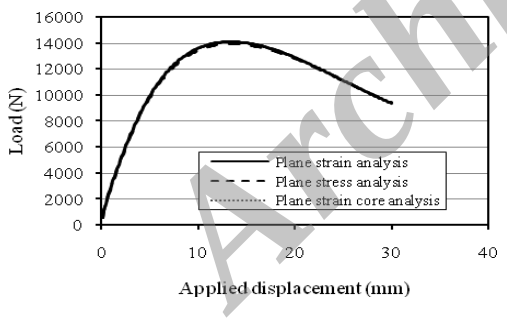

Fig. 11
Load-displacement variation for CZM analysis of the CT specimen for $\sigma_{\max}/\sigma_y = 1$.

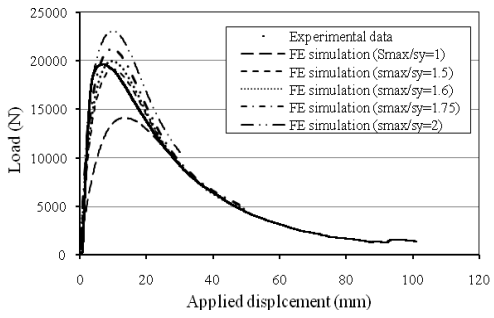

Fig. 12
Numerical load-displacement data calculated from cohesive zone model together with the experimental data.

To calibrate the CZM model as described in section 4, FE crack growth simulations incorporating Multi-linear Isotropic Hardening model were carried out using various relative cohesive strength ($\sigma_{\max}/\sigma_y$) and critical separation (δ_n) values. For each pair of trial values, an exponential cohesive law was derived and implemented to the interface contact elements. Comparison between numerical load-displacement responses with the experimental one would indicate the proper set of CZM parameters. The calculated critical fracture energy at the growth initiation (J_{Ic}), as explained in Section 5, is used in Eq. (8) as the work of separation. This work is used to define the separation of interface elements at the maximum stress (δ_n) for each assumed cohesive strength value ($\sigma_{\max}$). The trial relative cohesive strengths and their corresponding separations are given in Table 4. In order to investigate the dependency of the method to the constraints at the crack tip, the crack growth simulations have been performed with three plane stress, plane strain and plane strain core assumptions using $\sigma_{\max}/\sigma_y = 1$ and $\delta_n = 3.53$ mm. The results, as shown in Fig. 11, show that essentially no distinct difference exists in load-displacement variation for these three stress state assumptions. This also confirms that the CZM method is essentially independent of the constraint at the crack tip. However, the plane strain assumption is used for the rest of this simulation. The crack growth simulation for all the trial parameters, as given in Table 4. , was carried out. The numerical results together with the experimental data are shown in Fig. 12. The simulation results clearly indicate that the cohesive strength of 450 MPa ($\sigma_{\max}/\sigma_y = 1.6$) together with the critical separation value of 2.21 mm are reasonable values.

7 CONCLUSIONS

Stable ductile crack growth in 3 mm thick AISI 304 stainless steel specimens has been investigated experimentally and numerically. Tensile tests and finite element simulations have been performed to characterize the material and introduce a proper model for the material elasto-plastic response. CT fracture specimens have also been tested to generate load-displacement-crack growth data during stable crack growth. Subsequently, the critical fracture energy (J_{Ic}) was determined using a numerical solution.

In the present investigation, an attempt is made to tailor exponential CZM model for simulation of crack growth in CT specimens. The parameters of the model including maximum cohesive strength and corresponding separation were approximated using a finite element calibration method. On the basis of the study, the following conclusions can be made.

- Multi-linear Isotropic Hardening method in conjunction with the Von-Mises yield criterion is generally suitable to model the ductile behavior of the AISI 304 steel material provided adequate constraints applied to the analysis, i.e. plane stress analysis is quite inaccurate in this case.
- Exponential CZM model can be used successfully to model stable crack growth in this material.
- The CZM model parameters including the cohesive strength and critical material separation can be determined using elasto-plastic FE numerical simulations.
- Despite the fact that the material modeling is sensitive to the applied constraints, the CZM method is found to be quite insensitive to the applied constraints to the model. Therefore, the model can effectively be used in simulation of crack growth in AISI 304 steel components.

REFERENCES

[1] Kim J., Gao X., Srivatsan T.S., 2003, Modeling of crack growth in ductile solids: a three-dimensional analysis, *International Journal of Solids and Structures* **40**(26): 7357-7374.

[2] Wei Z., Deng X., Sutton M.A., Yang J., Cheng C. S., Zavattieri P., 2011, Modeling of mixed-mode crack growth in ductile thin sheets under combined in-plane and out-of-plane loading, *Engineering Fracture Mechanics* **78**(17): 3082-3101.

[3] Zhu X.K., Joyce J.A., 2012, Review of fracture toughness (G, K, J, CTOD, CTOA) testing and standardization, *Engineering Fracture Mechanics* **85**(1): 1-46.

[4] Pirondi A., Fersini D., 2009, Simulation of ductile crack growth in thin panels using the crack tip opening angle, *Engineering Fracture Mechanics* **76**(1): 88-100.

[5] Li H., Fu M.W., Lu J., Yang H., 2011, Ductile fracture: experiments and computations, *International Journal of Plasticity* **27**(2): 147-180.

[6] Jackiewicz J., Kuna M., 2003, Non-local requlariza tion for FE simulation of damage in ductile materials, *Computational Materials Science* **28**(3-4): 784-695.
[7] Barenblatt G.I., 1959, Equilibrium cracks formed during brittle fracture, *Journal of Applied Mathematics and Mechanics* **23**: 1273-1282.
[8] Dugdale D.S., 1960, Yielding of steel sheets containing slits, *Journal of the Mechanics and Physics of Solids* **8**: 100-104.
[9] Rahulkumar P., Jagota A., Bennison S.J., Saigal S., 2000, Cohesive element modeling of viscoelastic fracture: application to peel testing of polymers, *International Journal of Solids and Structures* **37**: 1873-1897.
[10] Siegmund T., Brocks W., 2000, A numerical study on the correlation between the work of separation and the dissipation rate in ductile fracture, *Engineering Fracture Mechanics* **67**: 139-154.
[11] Camacho G.T., Ortiz, M., 1996, Computational modeling of impact damage in brittle materials, *International Journal of Solids and Structures* **33**: 2899-2938.
[12] Mohammed I., Liechti K.M., 2000, Cohesive zone modeling of crack nucleation at bimaterial corners, *Journal of the Mechanics and Physics of Solids* **48**: 735-764.
[13] Roesler J., Paulino G.H., Park K., Gaedicke C., 2007, Concrete fracture prediction using bilinear softening, *Cement and Concrete Composites* **29**: 300-312.
[14] Shim D. J., Paulino G.H., Dodds Jr. R.H., 2006, J resistance behavior in functionally graded materials using cohesive zone and modified boundary layer models, *International Journal of Fracture* **13**: 91-117.
[15] Aronsson C.G., Backlund J., 1986, Tensile fracture of laminates with cracks, *Journal of Composite Materials* **20**: 287-307.
[16] Espinosa H.D., Dwivedi S., Lu H.C., 2000, Modeling impact induced delamination of woven fiber reinforced composites with contact/cohesive laws, *Computer Methods in Applied Mechanics and Engineering* **183**: 259-290.
[17] Song S.J., Wass A.M., 1995, Energy-based mechanical model for mixed-mode failure of laminated composites, *AIAA Journal* **33**: 739-745.
[18] Kubair D.V., Geubelle P.H., Huang Y.Y., 2003, Analysis of rate –dependent cohesive model for dynamic crack propagation, *Engineering Fracture Mechanics* **70**: 685-704.
[19] Liong R. T., 2011, *Application of the Cohesive Zone Model to the Analysis of Rotors with a Transverse Crack*, Karlsruher Institut Fur Technologie, KIT Scientific Publishing, Karlsruhe, Germany.
[20] Wang J.T., 2010, *Relating Cohesive Zone Models to Linear Elastic Fracture Mechanics*, NASA/TM-2010-216692, National Aeronautics and Space Administration, USA.
[21] Scheider I., Brocks W., 2003, Simulation of cup-cone fracture using the cohesive model, *Engineering Fracture Mechanics* **70**: 1943-1961.
[22] Cornec A., Schonfeld W., Schwalbe K. H., Scheider I., 2009, Application of the cohesive model for predicting the residual strength of a large scale fuselage structure with a two-bay crack, *Engineering Failure Analysis* **16**: 2541-2558.
[23] Li W., Siegmund T., 2002, An analysis of crack growth in thin-sheet metal via a cohesive zone model, *Engineering Fracture Mechanics* **69**: 2073-2093.
[24] Chen J., Fox D., 2012, Numerical investigation into multi-delamination failure of composite t-piece specimens under mixed-mode loading using a modified cohesive zone model, *Composite Structures* **94**(6): 2010-2016.
[25] Tvergaard V., Needleman A., 1984, Analysis of the cup-cone fracture in a round tensile bar, *Acta Metallurgica* **32**: 157-169.
[26] Needleman A., Tvergaard V., 1984, An analysis of ductile rupture in notched bars, *Journal of the Mechanics and Physics of Solids* **32**: 461-490.
[27] Li H., Chandra N., 2003, Analysis of crack growth and crack-tip plasticity in ductile materials using cohesive zone models, *International Journal of Plasticity* **19**: 849-882.
[28] Tvergaard V., 2001, Crack growth predictions by cohesive zone model for ductile fracture, *Journal of the Mechanics and Physics of Solids* **49**: 2191-2207.
[29] Geubelle P.H., Baylor J., 1998, Impact-induced delamination of laminated composites: a 2D simulation, *Composites* **29**: 589-602.
[30] Fernandes R.M.R.P., Chousal J.A.G., De Moura M.F.S.F., Xavier J., 2013, Determination of the cohesive laws of composite bonded joints under mode-II loading, *Composites Part B: Engineering* **52**: 269-274.
[31] Dourado N., Pereira F.A.M., De Moura M.F.S.F., Morais J.J.L., Dias M.I.R., 2013, Bone fracture characterization using the end notched flexure tests, *Materials Science and Engineerin C* **33**(1): 405-410.
[32] Zou Z., Reid S.R., Li S., 2003, A continuum damage model for delamination in laminated composites, *Journal of the Mechanics and Physics of Solids* **51**(2): 333-356.
[33] Xu X. P., Needleman A., 1993, Void nucleation by inclusion debonding in a crystal matrix, *Modeing and Simulation in Materials Science and Engineering* **1**: 111-132.
[34] Hsu C. L., Lo J., Yu J., Lee X. G., Tan P., 2003, Residual strength analysis using CTOA criteria for fuselage structures containing multiple site damage, *Engineering Fracture Mechanics* **70**: 525-545.
[35] James M.A., Newman Jr. J.C., 2003, The effect of crack tunneling on crack growth: experiments and CTOA analysis, *Engineering Fracture Mechanics* **70**: 457-468.
[36] Anandarajah A., 2010, *Computational Methods in Elasticity and Plasticity: Solids and Porous Media*, Springer Science International.